High-Performance Adaptive Torque Control for an IPMSM With Real-Time MTPA Operation

Qian Liu and Kay Hameyer, *Senior Member, IEEE*

***Abstract*—In this paper, a high-performance torque control scheme of an interior permanent magnet synchronous machine (IPMSM) is introduced, which focuses on both steady state and transient torque dynamics of the IPMSM under the maximum torque per ampere (MTPA) condition. For the proposed control scheme with model-based torque correction, an accurate and efficient torque control with robust torque response can be achieved for the MPTA operation. Global stability and performance of the proposed torque control scheme are theoretically guaranteed. The current limitation of the IPMSM is easily handled without anti-windup and without degrading the torque dynamics or stability even the torque demand is beyond the maximum reachable torque. Implementation issues of the proposed control scheme to the real IPMSM plant with parameter variation are discussed. With the compensation of the linear and nonlinear inverter voltage drop, a robust and accurate torque response for the real-time MTPA operation can be achieved by an adaptive current control and online parameter estimation. The simulation and experimental results validate the safety and high performance of the proposed torque control scheme.**

***Index Terms*—Adaptive torque control, current limitation, IPMSM, model reference adaptive system, real time MTPA, online parameter estimation, self torque correction, safety, transient dynamics.**

NOMENCLATURE

β	MTPA angle of current.
β^*	Reference MTPA angle with i_s^*.
$\hat{\boldsymbol{d}}$	Estimated disturbance voltage vector.
$\boldsymbol{d}$	Vector of disturbance voltages.
ϵ_d, ϵ_q	Model uncertainty in inverter and PMSM.
$\hat{\psi}_F$	Estimated flux linkage of PMSM.
$\hat{L}_d, \hat{L}_q$	Estimated d- and q-axis inductance.
$\hat{R}$	Estimated resistance of PMSM.
ψ_F	Flux linkage of PMSM.
ψ_{F0}	Nominal flux linkage of PMSM.
τ	Time constant of current closed loop.
d_d, d_q	Disturbance voltage in d- and q-axis.
f_{pwm}	Carrier frequency of inverter.
i_d, i_q	Current in d- and q-axis.
i_d^*, i_q^*	Reference current in d- and q-axis.
i_s	Amplitude of stator current.
$i_s^{'}$	Current amplitude out of torque correction.
i_s^*	Reference amplitude after limitation.
$i_{\max}$	Maximum current of PMSM.
k	Parameter of self-torque correction.
L_d, L_q	d- and q-axis inductance.
L_{d0}, L_{q0}	Nominal d- and q-axis inductance.
p	Pole pair number of PMSM.
R	Resistance of PMSM.
R_0	Nominal resistance of PMSM.
T_1	Electromagnetic torque of ideal PMSM.
T_2	Torque out of low pass filter.
T_e	Electromagnetic torque of PMSM.
$T_e^{'}$	Maximum torque at reference current i_s^*.
T_e^*	Reference torque.
t_{lin}	Linear delay of PMSM drive system.
$T_{\max}$	Maximum torque of PMSM.
t_s	Sampling time of controller.
t_{total}	Integrated time delay of inverter.
u_d, u_q	Voltage in d- and q-axis.
V_{DC}	DC-link voltage of inverter.
V_{err}	Nonlinear voltage distortion of inverter.

Manuscript received June 21, 2016; revised August 23, 2016 and October 6, 2016; accepted November 23, 2016. Date of publication December 1, 2016; date of current version May 18, 2017. Paper no. TEC-00530-2016.

The authors are with the Institute of Electrical Machines, RWTH Aachen University, Aachen 52056, Germany (e-mail: qian.liu@iem.rwth-aachen.de; kay.hameyer@iem.rwth-aachen.de).

Color versions of one or more of the figures in this paper are available online at http://ieeexplore.ieee.org.

Digital Object Identifier 10.1109/TEC.2016.2633302

I. Introduction

NOWADAYS the PMSM is very popular in industry applications. When compared to the other electrical machines, it has several advantages such as higher efficiency, higher torque density and better controllability. Since the PMSM is frequently used as the traction actuator, an efficient and high performance torque control is important for the PMSM. Different from the surface mounted PMSM (SPMSM), there is magnetic anisotropy in the IPMSM, which results in reluctance in the d- and q-axis. The torque of the IPMSM is not only produced by the synchronous torque from the q-axis current, but also by the reluctance torque from the d-axis current. An optimum combination of the the d- and q-axis current exists for the IPMSM to minimize the stator current for a fixed torque level. This optimum condition, named as MTPA, minimizes the copper losses of the IPMSM during the operation. On the other hand, the strong nonlinearity for the torque and current in the MTPA condition leads to the difficulty for a global high performance torque control.

The key point of the torque control under MTPA condition of the IPMSM is to obtain the reference current values for a given torque. In order to realize a real time MTPA operation, the optimum combination of the d- and q-axis currents should be found in real time. The constraint leading by the MTPA condition contains strong nonlinearity between the dq-axis currents

and the torque, which can be solved analytically by the Ferraris solution for the quartic equations [1]. However, a complicated recursive process is required to deal with the current limitation when the analytical solution of the MTPA condition is utilized.

Besides the analytical solution for the MTPA condition, the optimum reference current can be calculated online or offline by using the machine parameters and the MTPA equation [2]–[10]. For the offline procedure, the optimum reference dq-axis currents are numerically calculated offline at each torque level, which are stored in the look-up table (LUT) for the vector control [2]–[4]. The LUT approach requires accurately measured machine parameters for an accurate torque control. Therefore, the magnetic saturation and demagnetization of the PMSM lead to massive offline measuring and calculation when the LUT is implemented. The online procedure calculates the current reference using an outer loop controller and the MTPA condition [5]–[10]. In this approach, the nonlinear constraint for the current and torque under MTPA condition is loosed so that the reference dq-axis current vector can be obtained online without large computational cost [6]–[9]. In [10], a normalized torque-current relationship is introduced to reduce the real time calculation for the MTPA condition so that an accurate torque control can be realized. In [11], the nonlinearity of the MTPA condition can be reduced by a virtual factor to improve the performance of the controller.

Accurate machine parameters are required for the online tracking of the MTPA condition mentioned above to achieve the accurate torque control in real time. Both offline measured [6] and online estimated [7]–[10] of the machine parameters are convenient to be combined with the on-line calculation of the current reference. In order to realize a real time tracking of the machine parameters, different online estimation algorithm such as affine projection algorithm (APA) [7], recursive least square (RLS) [8], [9] and the model based low pass filter [12], [13] are introduced for the MTPA torque control. In order to ensure the estimated parameters to converge to the correct values, the rank-deficient problem should be avoided [14]. To prevent the ill condition for the estimation, most of the references assume part of the parameters of the PMSM plant to be constant [7], [8], [15]. Full estimations for all parameters of the PMSM are proposed with high frequency current injection in the d-axis [9], [14].

In recent years, a direct real time tracking of the MTPA condition is developed based on the extremum seeking control with signal injection (ESC) [16]–[19] or virtual signal injection [20]. This online tracking is independent on parameters so that no parameter estimator is required. However, this approach focus on efficient control instead of accurate torque control [10]. On the other hand, in most of the aforementioned control schemes, the safety, stability and transient torque dynamics for the torque control under MTPA condition are not considered, especially with parameter mismatch. In [21], the idea for the torque dynamics of the PMSM with MTPA operation using self-torque correction is mentioned. However, it lacks both theoretically proof for the general stability and robustness and the experimental validation.

This paper focuses on a high performance adaptive self-torque correction scheme with real time MTPA operation, which is an extension of [21] with both theoretical and practical improvements. Compared to the aforementioned existing torque control schemes under MTPA condition, the proposed control scheme can achieve both efficient and accurate torque control simultaneously with high level robustness and satisfactory transient dynamics. An online RLS parameter estimator is embedded in the proposed control scheme for the real time accurate torque control with MTPA condition. When compared to [21], a more general self-torque correction scheme is proposed in this paper to ensure the fast dynamics of the torque. Besides, completely theoretical proofs for general stability and performance of the torque controller with current limitation and parameter mismatch, which are the essential and critical parts for the controller design, are given in this paper. Moreover, the implementation issues of the proposed control scheme to the real PMSM drive system such as the linear and nonlinear effects of the inverter are considered to guarantee the feasibility and effectiveness. Both simulation and experimental results validate the high performance of the proposed control scheme.

II. Model of the PMSM

The model of a 3-phase PMSM can be described in the synchronous dq reference frame using amplitude invariant Park Transformation, which is shown by the following equations:

$$u_d = Ri_d + L_d\frac{di_d}{dt} - \omega L_q i_q + \epsilon_d \tag{1}$$

$$u_q = Ri_q + L_q\frac{di_q}{dt} + \omega(L_d i_d + \psi_F) + \epsilon_q \tag{2}$$

$$T_e = \frac{3p}{2}(\psi_F + (L_d - L_q)i_d)i_q, \tag{3}$$

where R, L_d, L_q and ψ_F denote the real stator resistance, inductances and the magnetic flux linkage of the PMSM respectively. p is the pole pair number. Since the inverter is non-ideal voltage source for the PMSM and contains nonlinear voltage distortion, the impact of uncertainties from the inverter has to be considered into the system model of the PMSM drive system for the controller design. The ϵ_d and ϵ_q denote the model uncertainties such as the inverter effects and high order harmonics without loss of generality. However, this paper is not aimed for the torque ripple reduction so that the high order harmonics and cogging torque are not specifically considered. Considering the parameter variation, the model of the PMSM (1) (2) can be reformed into a general form, which is convenient for the controller design [22]:

$$\dot{\boldsymbol{i}} = \boldsymbol{A_0 i} + \boldsymbol{B_0}(\boldsymbol{u_s} + \boldsymbol{u_e} - \boldsymbol{d}), \tag{4}$$

where the parameters and variables in eq. (4) are defined as:

$$\boldsymbol{i} = \begin{bmatrix} i_d \\ i_q \end{bmatrix},\ \boldsymbol{u_s} = \begin{bmatrix} u_d \\ u_q \end{bmatrix},\ \boldsymbol{u_e} = \begin{bmatrix} \omega L_{q0} i_q \\ -\omega(L_{d0} i_d + \psi_{F0}) \end{bmatrix},$$

$$\boldsymbol{d} = \begin{bmatrix} d_d \\ d_q \end{bmatrix},\ \boldsymbol{A_0} = \begin{bmatrix} -\frac{R_0}{L_{d0}} & 0 \\ 0 & -\frac{R_0}{L_{q0}} \end{bmatrix},\ \boldsymbol{B_0} = \begin{bmatrix} \frac{1}{L_{d0}} & 0 \\ 0 & \frac{1}{L_{q0}} \end{bmatrix}.$$

Here R_0, L_{d0}, L_{q0} and ψ_{F0} are the fixed nominal parameters of the PMSM. The vector $\boldsymbol{d} = [d_d,\ d_q]^T$ is an integrated model error in both d- and q-axis, which varies with the operating

condition and is unmeasurable. The detailed expression of $\boldsymbol{d}$ can be described by the following equations [22]:

$$d_d = \Delta R i_d + \Delta L_d \frac{di_d}{dt} - \Delta L_q \omega i_q + \epsilon_d, \tag{5}$$

$$d_q = \Delta R i_q + \Delta L_q \frac{di_q}{dt} + (\Delta L_d i_d + \Delta \psi_F)\omega + \epsilon_q, \tag{6}$$

where $\Delta R = R - R_0$, $\Delta L_d = L_d - L_{d0}$, $\Delta L_q = L_q - L_{q0}$ and $\Delta\psi_F = \psi_F - \psi_{F0}$. The model (4) contains all the system uncertainty without loss of generality.

By neglecting the system uncertainty in the PMSM drive system ($\boldsymbol{d} = 0$), the basic vector controller of the PMSM is realized by a PI controller:

$$u_d^* = \frac{L_{d0}}{\tau} E_d + \frac{R_0}{\tau} \int E_d dt - \omega L_{q0} i_q, \tag{7}$$

$$u_q^* = \frac{L_{q0}}{\tau} E_q + \frac{R_0}{\tau} \int E_q dt + \omega (L_{d0} i_d + \psi_{F0}), \tag{8}$$

where $E_d = i_d^* - i_d$ and $E_q = i_q^* - i_q$. $*$ stands for the reference value. The closed loop systems for the d- and q-axis with vector control can be approximated by a low pass filter:

$$i_d(s) = \frac{1}{1+\tau s} i_d^*(s) \tag{9}$$

$$i_q(s) = \frac{1}{1+\tau s} i_q^*(s), \tag{10}$$

The time constant τ is the adjustable time constant, which determines the frequency bandwidth of the closed current loop.

III. MTPA Torque Control with Self-Correction

The proposed torque control with MTPA condition designed based on the ideal model of the IPMSM at first, which is by neglecting the system uncertainty and parameter variation. The following two assumptions are made in this section to simplify the introduction of the proposed torque control scheme:

1) the parameters of the IPMSM are considered as known constants: $\Delta L_d = \Delta L_q = \Delta\psi_F = 0$.
2) the current dynamics (9) and (10) are always true.

According to equation (3), with the reluctance $L_d - L_q$, minimum copper losses of the IPMSM can be realized with an optimum current vector for the desired electromagnetic torque. Denote β as a phase angle of the stator current $\boldsymbol{i_s}$. The MTPA condition is reached at a global extreme for the torque T_e and the phase angle β:

$$\frac{\partial T_e}{\partial \beta} = \frac{3p}{2}[(L_q - L_d) i_s^2 \cos(2\beta) - \psi_F i_s \sin(\beta)] = 0 \tag{11}$$

$$i_d = -i_s \sin(\beta), \quad i_q = i_s \cos(\beta). \tag{12}$$

By solving the MTPA constraint (11), the relation between $i_s = \sqrt{i_d^2 + i_q^2}$ and the angle β can be obtained [9]:

$$\beta = \sin^{-1}\left(\frac{-\psi_F + \sqrt{\psi_F^2 + 8(L_q - L_d)^2 i_s^2}}{4(L_q - L_d) i_s}\right). \tag{13}$$

The relation of the torque and current (3), (12) and (13) contains strong nonlinearity between the torque and the stator current. Therefore, it is costly to determine i_s and β simultaneously and analytically for a given torque. On the other hand, if a outer loop controller is introduced to produce the current reference, it is difficult to design a PI torque controller which guarantees the global stability and performance due to the nonlinearity [11].

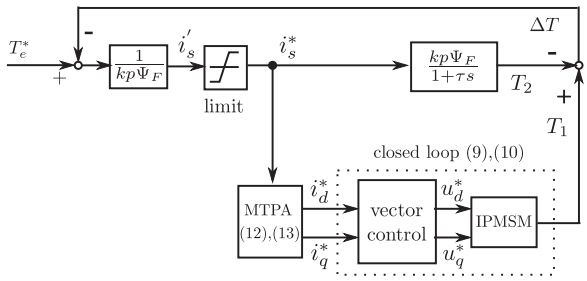

Fig. 1. Torque control with MTPA using model tracking.

To achieve a high performance torque control with MTPA condition, a control scheme shown in Fig. 1 is designed for an ideal IPMSM drive system under assumptions 1) and 2). In the figure, p is the pole pair number and $k \leq 1.5$ is a constant controller parameter determining the torque dynamics. Using the torque equation (3) and the current dynamics (9) (10), the torque T_1 of a well current controlled IPMSM with MTPA condition can be described as a second order linear system [21]:

$$\tau^2 \ddot{T}_1 + 3\tau \dot{T}_1 + 2T_1 = 2T_e', \tag{14}$$

here T_1 is the torque of the PMSM plant, T_e' is defined by

$$T_e' = \frac{3p}{2}[\psi_F + (L_q - L_d) i_s^* \sin(\beta^*)] \cos(\beta^*) i_s^*. \tag{15}$$

Here β^* is the corresponding optimum current phase angle with the stator current i_s^*. With the torque dynamics (14), a self-correction process is utilized to obtain the optimum reference current i_s^* for a high performance torque control, which is shown in Fig. 1. A low pass filter is inserted for the model based torque correction with following transient dynamics:

$$\tau \dot{T}_2 + T_2 = T_e^+ \tag{16}$$

$$T_e^+ = \begin{cases} kp\psi_F \text{sign}(i_s') i_{\max} & \text{if} |i_s'| > i_{\max} \\ T_e^* - \Delta T & \text{otherwise} \end{cases} \tag{17}$$

$$\Delta T = T_1 - T_2 = T_e^* - kp\psi_F i_s', \tag{18}$$

where τ is the time constant of the current closed loop and T_2 is the torque response out of the low pass filter in Fig. 1. $i_{\max}$ is the maximum amplitude of the stator current. T_e^* is the desired reference torque. Since the cases $i_s' \leq 0$ and $i_s' \geq 0$ are symmetrically the same, only the discussion for $i_s' \geq 0$ is shown here. Denote $T_{\max}$ as the maximum reachable torque due to the current limitation $i_{\max}$. To discuss the dynamics of the torque, the following Lemma is proven.

Lemma 3.1: If neglecting the current limitation, the reference current i_s^* converges asymptotically to its optimum value for the MTPA condition, which is the equilibrium point of the nonlinear equation $T_e' = T_e^*$. Meanwhile, the torque T_e' converges to the reference value T_e^* asymptotically with the convergence time fast than or equal to $\frac{k}{1.5}\tau$.

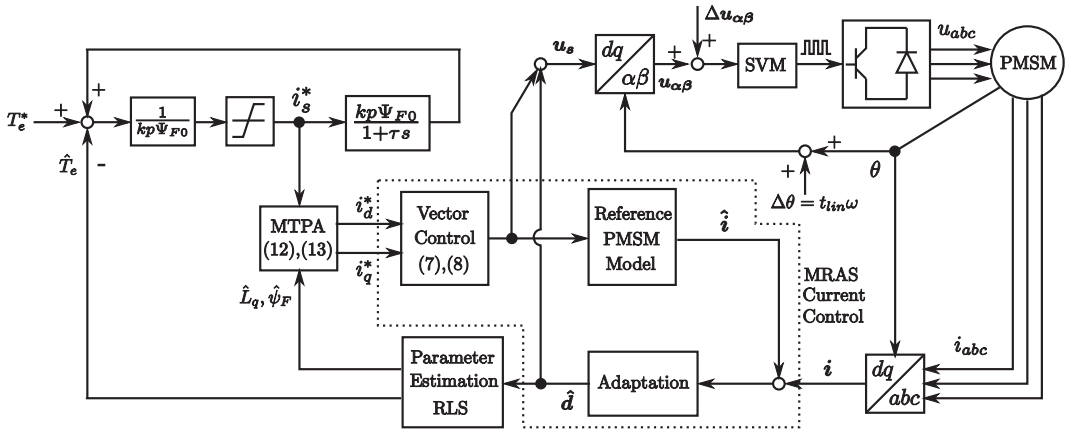

Fig. 2. Proposed adaptive torque structure with MTPA self-correction.

The proof of Lemma 3.1 is shown in Appendix VII-A, which is a more general case when compared to the conclusion in [21]. From Lemma 3.1, when the current limitation is not reached and $k \leq 1.5$ holds, the convergence time $\frac{k}{1.5}\tau$ for the torque $T_e^{'}$ to T_e^* can be much faster than the one for T_1 to $T_e^{'}$ in eq. (14). Consequently, the transient dynamics that $T_e^{'}$ converges to T_e^* can be considered as a fast inner loop for the torque dynamics (14) of the IPMSM. Therefore, the torque T_1 converges to the its reference T_e^* with guaranteed transient performance.

Considering the current limitation, when the current $i_s^{'}$ exceeds the maximum allowed current $i_s^{'} > i_{\max}$, $i_s^* = i_{\max}$ and $T_e^{'} = T_{\max}$. Using equations (14) and (16), the following equation holds:

$$\tau^2 \dddot{i}_s^{'} + 3\tau \ddot{i}_s^{'} + 2\dot{i}_s^{'} = 2i_s^+$$
$$i_s^+ = i_{\max} + \frac{T_e^* - T_{\max}}{kp\psi_F}. \tag{19}$$

Here i_s^+ in eq. (19) is a constant. $i_s^{'}$ converges asymptotically towards the value i_s^+ with the same convergence rate that the torque T_1 converges to $T_e^{'}$. If the desired torque $T_e^* > T_{\max}$, the current $i_s^{'}$ is larger than $i_{\max}$ and $i_e^* = i_{\max}$. In this case, $T_e^{'} = T_{\max}$ always holds and T_1 converges to the maximum torque $T_{\max}$ asymptotically. On the other hand, if $T_e^* < T_{\max}$, it can be divided in to two stages. In the first stage, $i_s^{'}$ reduces according to the convergence rate that the torque T_1 converges to $T_e^{'}$ until it reaches $i_s^{'} = i_{\max}$. Then $i_s^{'}$ converges to its optimum value within the current limitation and $T_e^{'}$ converges to T_e^* according to Lemma 3.1. In this case, the convergence rates of both stages are faster than or equal to the one that T_1 converges to $T_e^{'}$. Therefore, the transient dynamics that $T_e^{'}$ converges to T_e^* is still a fast inner loop for the torque dynamics (14) of the IPMSM, which guarantees the transient performance of the torque T_1.

With the discussion above, it can be concluded that when the assumptions 1) and 2) are fulfilled, the torque control scheme for MTPA operation in Fig. 1 has guaranteed steady state and transient torque performance. The current amplitude i_s^* and the corresponding phase angle β^* converge to the optimum values of the MTPA condition for the given torque T_e^*. Therefore, both MTPA condition and high performance torque control can be achieved. The current limitation is easily handled without any additional adjustment of the reference torque T_e^* such as anti-windup. When the reference torque T_e^* can not be reached, the current and the torque of the IPMSM will stay at their maximum reachable values without stability problem. On the other hand, the current limitation has limited influence on the torque dynamics.

IV. Implementation on the Real IPMSM with Parameter Variation

The self-correction torque control described in Section III can achieve a high performance torque dynamics for the IPMSM with parameter variation. The key point is that the two assumptions 1) and 2) in Section III are fulfilled for the real IPMSM drive system. It can be noticed, when the assumption 1) is realized, the accurate current phase angle is calculated for the real MTPA condition. The assumption 2) is to ensure the torque dynamics of the IPMSM. For assumption 2), an adaptive current control using model reference adaptive system (MRAS) can enforce the closed current loop to behave as a low pass filter which described in (9) and (10). The assumption 1) can be realized by a fast online parameter estimation or stored LUT of the machine parameters for different operating conditions. Therefore, both assumptions in Section III can be fulfilled for the implementation in the real IPMSM drive system. Therefore, the high performance torque control for the IPMSM with real time MTPA condition can be realized. In this paper, online parameter estimation is utilized to fulfill assumption 1). The proposed torque control scheme for the real IPMSM with parameter variation is shown in Fig. 2. According to the proof of Lemma 3.1, the constant k is chosen with the boundary $k \leq 1.5\frac{\psi_{F,\min}}{\psi_{F0}}$ to ensure that the convergence rate of torque reference T_e^* is faster than the one of the current closed loop. Here $\psi_{F,\min}$ denotes the lower bound of the flux linkage of the IPMSM during the operation. Moreover, a small k leads to fast convergence of the reference torque and therefore the fast dynamics of the torque T_e. However, the k can not be too small considering the noise in the estimation and measurement. The optimum k

can be determined by tuning in the experiments to trade-off the torque dynamics and noise level.

A. Adaptive current control using MRAS

The block diagrams which are enclosed by the dashed line in Fig. 2 present the adaptive current controller. The detailed design and analysis of the current controller and the description of the variables in Fig. 2 for the current controller can be found in [21] and [23]. With the adaptive current controller, the current loop of the IPMSM plant performs approximately in the same way as the desired low pass filter (9) and (10). Since all the parameter mismatch are considered within the the integrated system disturbance $\boldsymbol{d}$, the parameter mismatch such as saturation and cross-coupling has very limited influence on the performance of the adaptive current controller, if the dynamics of the adaptation process is designed fast enough. Meanwhile, the integrated system disturbance $\boldsymbol{d}$ can be estimated according to the adaptation procedure.

B. Digital signal processor (DSP) and inverter effect

For accurate parameter estimation, the current and terminal voltage of the IPMSM plant are required for the estimation algorithm. In the real PMSM drive system, no voltage sensor is provided to measure the terminal voltage of the PMSM out of the inverter. Instead, the voltage $\boldsymbol{u_s}$ out of the current controller is utilized. Therefore, the voltage distortion between the reference voltage out of the current controller and the real voltage of the PMSM out of the inverter, which is caused by the DSP and inverter, has to be compensated.

Neglecting the high order harmonics, the main effects of the DSP and the inverter are composed by several time delays on the phase voltages [24]: the turn-on time $t_{\rm on}$, turn-off time $t_{\rm off}$ and the artificially imposed delay t_d of the IGBT during the transition; sampling delay of the voltage due to the space vector modulation $t_{\rm svm}$; delay due to the current measuring $t_{\rm meas}$ such as filtering delay; calculation delay of the DSP $t_{\rm dsp}$. These time delays result in both linear delay and nonlinear voltage drop on the voltage $\boldsymbol{u_s}$ out of the current controller. The nonlinear voltage drop $V_{{\rm err},j}$, $j=a,b,c$ in each phase is caused by the $t_{\rm on}$, $t_{\rm off}$ and t_d, which can be estimated by an integrated time delay $t_{\rm total}$ [25]:

$$\begin{aligned} V_{{\rm err},j} &= V_j^* - V_j \\ &\approx \left[\frac{V_s + V_d}{2} + \frac{V_j^*}{V_{DC}} + V_{DC} f_{\rm pwm} t_{\rm total}\right] {\rm sign}(i_j), \end{aligned} \tag{20}$$

where V_j^* and V_j denote the reference and real voltage on phase j ($j=a,b,c$). i_j is the measured current of phase j. V_d and V_s are the diode and IGBT forward voltages respectively. V_{DC} is the DC-link voltage of the inverter. $f_{\rm pwm}$ is the carrier frequency of the inverter. The integrated time delay $t_{\rm total}$ can be measured and stored in the look-up table by using the method described in [25]. The voltage drop $\Delta\boldsymbol{u_{\alpha\beta}}$ in the $\alpha\beta$ coordinate system is calculated by:

$$\Delta\boldsymbol{u_{\alpha\beta}} = \frac{2}{3}\begin{bmatrix} 1 & -\frac{1}{2} & \frac{1}{2} \\ 0 & \frac{\sqrt{3}}{2} & -\frac{\sqrt{3}}{2} \end{bmatrix} \begin{bmatrix} V_{{\rm err},a} \\ V_{{\rm err},b} \\ V_{{\rm err},c} \end{bmatrix}. \tag{21}$$

The estimated nonlinear voltage drop $\Delta\boldsymbol{u_{\alpha\beta}}$ is compensated in the control scheme according to Fig. 2.

The linear delay of the DSP and inverter can be integrated by one single time constant $t_{\rm lin}$, which is calculated by $t_{\rm lin} = t_{\rm svm} + t_{\rm meas} + t_{\rm dsp}$. For the symmetrical SVM, the time delay of the voltage sampling $t_{\rm svm}$ due to the zero-order-holder is $1/(2f_{\rm pwm})$. The delay due to the calculation of the digital processor $t_{\rm dsp}$ is one period of the sampling time of the digital controller t_s, which is $t_{\rm dsp} = t_s$. The delay due to the current measuring $t_{\rm meas}$ depends on the interruption delay of the current measurement and the frequency band of the low pass filter, which can be different according to the configuration of the drive system. The linear delay $t_{\rm lin}$ results in the phase lag $\Delta\theta = t_{\rm lin}\omega$ on the voltage, which can be compensated by the dq to $\alpha\beta$ transformation in Fig. 2.

C. Estimation of the parameters and torque

To achieve an accurate torque control and the real MTPA operation, the real time parameters of the IPMSM should be updated to the calculation of the phase angle β^* in eq. (13) for the corresponding current reference i_d^* and i_q^*. The optimum phase angle β^* is based on the estimated inductances L_d, L_q and the flux linkage ψ_F, which are current dependent in the IPMSM. On the other hand, the ohmic resistance R and the flux linkage ψ_F vary with the temperature. However, for secure parameter estimation without potential rank-deficient problem, two parameters can be estimated online for the PMSM without extra signal injection. The relationship between the resistance R and the temperature is described by the following equation:

$$R = R_{T0}(1 + \alpha(T - T_0)). \tag{22}$$

where R_{T0} is the resistance at the temperature T_0. α is the temperature coefficient of the resistance. For the copper windings, the coefficient $\alpha = 3.93 * 10^{-3}/C^\circ$, which is very small. The temperature increment is limited by the cooling and the resistance of the IPMSM varies slow with the temperature. On the other hand, for the high efficiency PMSM, the resistance R is small. It has limited influence on the behavior of the PMSM when the speed is above a certain level. Therefore, the stator resistance R is considered as a constant in this paper.

Since the magnetic path in the d-axis is much longer than the one in q-axis for the IPMSM. The variation of L_d due to the saturation is much smaller than the one on L_q [1], [15]. In [26], it shows that the variation of L_d is very small for different rotor topologies considering cross-coupling effect. Fig. 3 shows the measured saturation effects of L_d and L_q for an IPMSM depending on different current levels. It can be noticed that the saturation effect on L_d is very small. On the other hand, the variation range of the q-axis current i_q is larger than the one of the d-axis current i_d in the IPMSM for the MTPA operation.

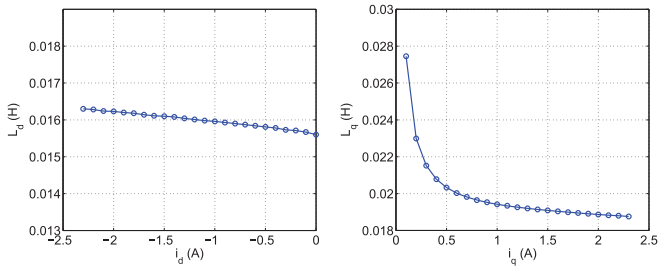

Fig. 3. Measured inductances L_d and L_q with varying current.

TABLE I
PARAMETERS OF THE IPMSM

Rated current	$i_{\max}$	2.3 A
Rated torque	$T_{\max}$	1.23 Nm
DC-link voltage	V_{DC}	60 V
Rated speed (mechanical)	$\omega_{m,N}$	500 rpm
Pole pair number	p	4
Stator resistance	R_s	3.3Ω
d-axis inductance	L_d	16 mH
q-axis inductance	L_q	20 mH
Flux linkage	ψ_F	0.0886 Vs/rad

The flux linkage ψ_F has the dominant influence on the torque dynamics. Therefore, L_d can be considered as a constant in order to avoid the rank deficient problem for the parameter estimation.

The RLS algorithm is utilized in this paper to estimated the q-axis inductance L_q and the flux linkage ψ_F. The RLS with a forgetting factor compromises the convergence rate and the noise level of the estimated parameters. The RLS algorithm is described by the following equations:

$$\hat{\boldsymbol{\theta}}(n) = \hat{\boldsymbol{\theta}}(n-1) + \boldsymbol{K}(n)(\boldsymbol{y}(n) - \boldsymbol{\varphi}^{\boldsymbol{T}}(n)\hat{\theta}(n-1))$$
$$\boldsymbol{K}(n) = \boldsymbol{P}(n-1)\boldsymbol{\varphi}(n)(\lambda \boldsymbol{I} + \boldsymbol{\varphi}^{\boldsymbol{T}}(n)\boldsymbol{P}(n-1)\boldsymbol{\varphi}(n))^{-1}$$
$$\boldsymbol{P}(n) = \frac{1}{\lambda}(\boldsymbol{I} - \boldsymbol{K}(n)\boldsymbol{\varphi}^{\boldsymbol{T}}(n))\boldsymbol{P}(n-1),$$

where $\boldsymbol{y} = \boldsymbol{\varphi}^{\boldsymbol{T}}\boldsymbol{\theta}$ is the system description. $\boldsymbol{y}$ and $\boldsymbol{\varphi}$ are the outputs and states; $\boldsymbol{\theta}$ and $\hat{\boldsymbol{\theta}}$ are the real and estimated parameter vectors respectively. λ is a positive forgetting factor, which is chosen less than 1 and presents the trade-off between convergence rate and the noise filtering.

In the proposed control scheme, the estimated system disturbance from the adaptive current controller, which is denoted by $\hat{\boldsymbol{d}}$, is utilized to estimated L_q and ψ_F. According to the adaptive control, the estimated system disturbance $\hat{\boldsymbol{d}}$ tracks the real value $\boldsymbol{d}$ fast enough so that $\hat{\boldsymbol{d}} = \boldsymbol{d}$ can be assumed. The advantage of using $\hat{\boldsymbol{d}}$ instead of $\boldsymbol{u_s}$ is to reduce the influence of the transient dynamics di_d/dt to the parameter estimation. Since the inverter and DSP effects are compensated in the control scheme, the system disturbance $\boldsymbol{d}$ only contains the voltage error caused by the parameter variation of the IPMSM. Considering equations (5) (6) by by assuming $\Delta R = 0$ and $\Delta L_d = 0$, the following discrete system can be obtained:

$$\begin{bmatrix} t_s d_d(n) \\ t_s d_q(n) \end{bmatrix} = \begin{bmatrix} -t_s \omega i_q(n) & 0 \\ i_q(n) - i_q(n-1) & t_s \omega \end{bmatrix} \begin{bmatrix} \Delta L_q \\ \Delta \psi_F \end{bmatrix}. \quad (23)$$

Equation (23) is directly applied to the RLS algorithm. The estimation considering the current difference $i_q(n) - i_q(n-1)$ can increase the convergence rate of the estimated parameters [21]. Using the estimated parameter variation $\Delta\hat{L}_q$ and $\Delta\hat{\psi}_F$ with RLS algorithm, the real time q-axis inductance and the flux linkage can be obtained by $\hat{L}_q = L_{q0} + \Delta\hat{L}_q$ and $\hat{\psi}_F = \hat{\psi}_{F0} + \Delta\hat{\psi}_F$. The estimated torque $\hat{T}_e$ of the PMSM is obtained by the equation (24) using the estimated machine parameters.

$$\hat{T}_e = \frac{3p}{2}(\hat{\psi}_F + (\hat{L}_d - \hat{L}_q)i_d)i_q. \quad (24)$$

D. Influence of the inaccurate machine parameters

Due to the imperfect compensation of the inverter effect and the resistance increment, it is possible that the estimated parameters of the PMSM are deviated from their real values at low speed. However, the assumption 2) in Section III can always be achieved since the current control loop using MRAS is parameter independent. In this case, taking the derivative of equation (24), the dynamics of the estimated torque $\hat{T}_e$ can be described by the following equation:

$$\tau^2\ddot{\hat{T}}_e + 3\tau\dot{\hat{T}}_e + 2\hat{T}_e = 2T_e^{''}, \quad (25)$$

where $T_e^{''}$ is calculated by the estimated parameters:

$$T_e^{''} = \frac{3p}{2}[\hat{\psi}_F + (\hat{L}_q - \hat{L}_d)i_s^* \sin(\beta^*)]\cos(\beta^*)i_s^*. \quad (26)$$

Equations (25) and (26) have the same form as equations (14) and (15). Using the same proof for the Lemma 3.1, it can be concluded that the torque $T_e^{''}$ converges asymptotically to T_e^* without the current limitation and the reference current i_s^* converges to the solution of the equation $T_e^{''} = T_e^*$ asymptotically. The convergence time of $T_e^{''}$ to T_e^* is faster than or equal to $k\frac{\tau\psi_{F0}}{1.5\psi_F}$. Similar with the analysis in Section III, the inaccurate machine parameters have no impact on the stability of the system and limited influence on the torque dynamics. However, the current reference may deviate from the MTPA condition and steady state torque error may exist due to the inaccurate parameters. For the dynamic torque response, only the flux linkage drop slows down the convergence rate of the torque when compared to the case without parameter error. However, a sufficiently small coefficient k can be chosen to guarantee the convergence rate of $T_e^{''}$.

V. SIMULATION RESULTS

The simulation model is implemented in Matlab/Simulink to validate the theoretical statements of the torque dynamics for the proposed control scheme. The parameters of the IPMSM are collected in Table I. The controller is implemented as the a digital controller. The sampling frequency for the controller and the switching frequency of the inverter is 8 kHz. A symmetric SVM is applied to the inverter. In the simulation, the inverter

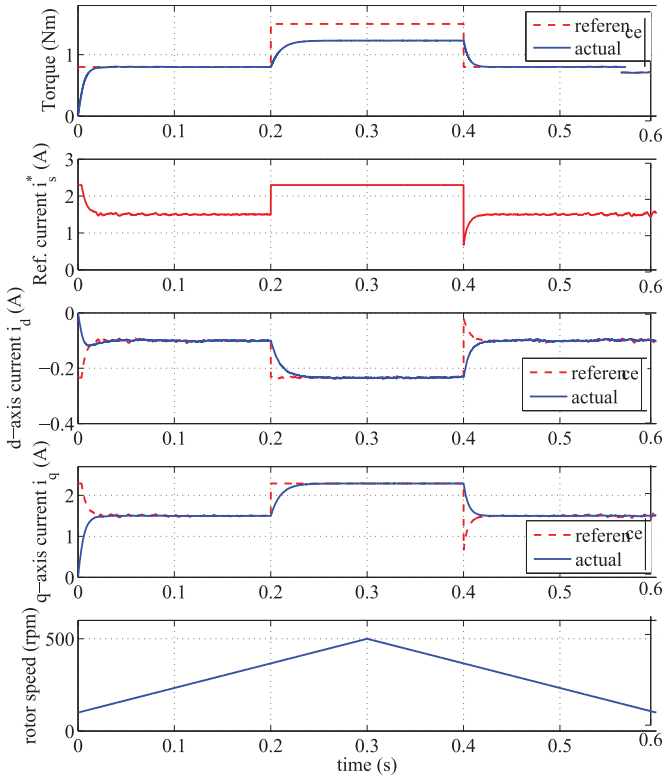

Fig. 4. Simulation results without parameter error of the IPMSM.

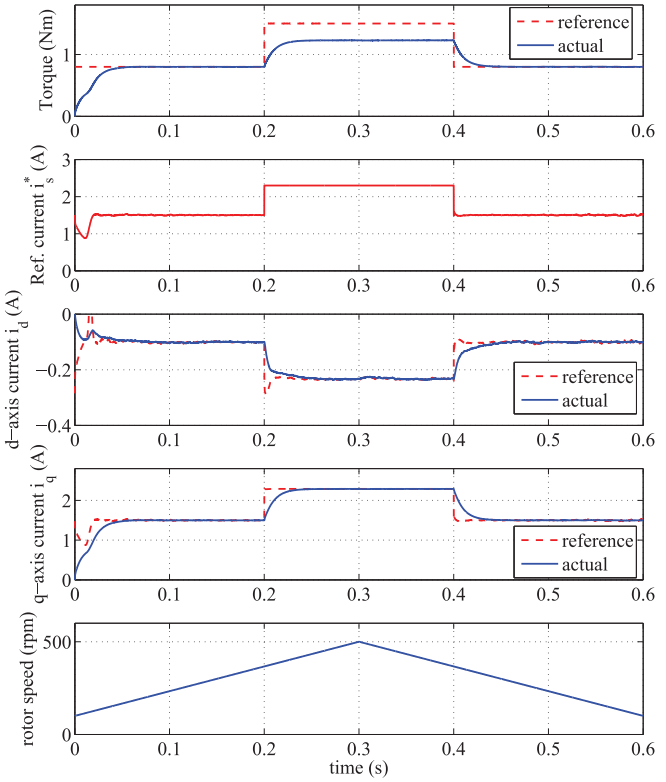

Fig. 5. Simulation results with inductance and flux linkage errors: $L_{q0} = 2L_q$ and $\psi_{F0} = 2\psi_F$.

and the IPMSM plant are simulated as continuous systems by using a step size 0.3125 μs, which is much smaller than the sampling time of the controller. The current and speed are measured by the zero-order-holder at 8 kHz. The time constant of the inner current loop is chosen to $\tau = 0.01$ s. In this paper, the lower bound of the flux linkage ψ_F is set to $\frac{1}{2}\psi_{F0}$. According to the analysis in Section IV, the constant k is chosen to 0.75. The speed of the IPMSM vary from 100 rpm to its rated value 500 rpm. In the real case, the parameters of the IPMSM plant can not be artificially manipulated. Therefore, the nominal parameters are chosen to different values to emulate different situations with and without parameter mismatch in both sections for simulations and experiments.

Fig. 4 shows the simulation results without parameter mismatch of the IPMSM, which is $R_0 = R$, $L_{d0} = L_d$, $L_{q0} = L_q$ and $\psi_{F0} = \psi_F$ for the nominal parameters. It can be noticed that the reference current i_s^* as well as the i_d^* and i_q^* converge to the optimum values of the MTPA condition asymptotically, which validates the theoretical conclusions in Section III. The torque of the IPMSM T_e approaches to the reference value asymptotically. When the torque reference is unreachable, the torque T_e stays at the maximum torque while the stator current i_s^* is limited to its maximum value.

In Fig. 5, the simulation results of the torque and current are shown with inductance and flux linkage error: $L_{q0} = 2L_q$ and $\psi_{F0} = 2\psi_F$. The chosen nominal parameters $L_{q0} = 2L_q$ and $\psi_{F0} = 2\psi_F$ represents 50% inductance drop due to saturation effect and 50% flux linkage drop respectively. The estimated parameters are shown in Fig. 6. It can be noticed that the

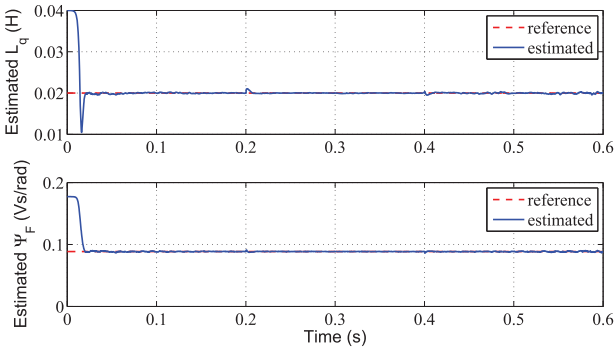

Fig. 6. Estimated parameters with inductance and flux linkage errors: $L_{q0} = 2L_q$ and $\psi_{F0} = 2\psi_F$.

parameter errors result in small influence on the torque and current dynamics. The estimated L_q and ψ_F converge to the correct values in a short time. Before the estimated L_q and ψ_F are stabilized, the convergence of the current and torque is slowed down. However, due to the short time convergence of the estimated parameters, the performance of the torque and current are still satisfied. After the estimated L_q and ψ_F are stabilized, the torque and current of the IPMSM perform as well as without parameter errors.

In order to show the effectiveness of the self-torque correction, the simulated torque response of the torque control with and without self-torque correction are shown in Fig. 7. Both cases are simulated without parameter mismatch of the IPMSM. For the case without self-torque correction, the feedback torque

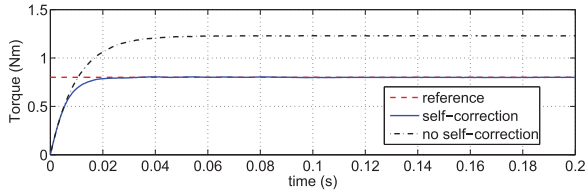

Fig. 7. Simulation results of torque response with and without self-torque correction.

correction ΔT in Fig. 1 is removed, while the current control loop remains unchanged for a fair comparison. It is shown in Fig. 7 that without the self-torque correction, the torque of the IPMSM deviates far from the desired reference torque.

VI. Experimental Results

In order to show the feasibility and the performance of the proposed control scheme in the real IPMSM drive system, several experiments are made for the IPMSM with parameters in Table I. The offline measured L_d at $i_q = 2$ A and L_q at $i_d = -0.3$ A due to the saturation effect are shown in Fig. 3. The cross coupling effect of the test IPMSM is shown by Fig. 15 in Appendix VII-B after 3D finite element analysis. The cross coupling effect is very small and therefore can be neglected. The controller is implemented in the dSPACE rapid control prototyping system (DS1103). The configuration of the controller in the experiments is set as the same as the one for the simulation in Section V. The speed of the IPMSM is controlled to 300 rpm by a load machine. In the experiments, the accuracy of the torque control is verified by the its mean value, while the accuracy of the MTPA condition is shown by the accuracy of the estimated parameters.

Fig. 8 and fig. 9 show the experimental results for the controller with nominal parameters which equal to the one in Table I. It is approximately the case without parameter errors. From these figures, it can be noticed that the performance of the current and torque coincides the theoretical conclusion. In Fig. 8, the reference current i_s^* converges to the optimum value under MTPA condition asymptotically so that the torque T_e of the IPMSM approaches to 1 Nm with high performance. The mean value of T_e stays at 1 Nm in steady state, which shows the accuracy of the torque. The estimated L_q in steady state is 19.35 mH at $i_q = 1.88$ A, which is with 2.3% displacement from the offline measured value 18.92 mH. The estimated ψ_F is 0.0881 Vs/rad. In Fig. 9, when the torque reference is unreachable, The current stays at the maximum current as well as the mean value of torque T_e stays at the maximum reachable value 1.23 Nm without degrading the system stability and the torque dynamics. The estimated L_q in steady state is 18.7 mH at $i_q = 2.29$ A, which has less than 1% error from the offline measured value 18.74 mH.

Fig. 10 and fig. 11 show the experimental results with parameter error $L_{q0} = 40$ mH, which is approximately double of the real q-axis inductance L_q. In Fig. 10, it can be noticed, with the proposed self torque correction, the system is stable with smooth torque response when using the wrong inductance of the IPMSM. Therefore, the control scheme is

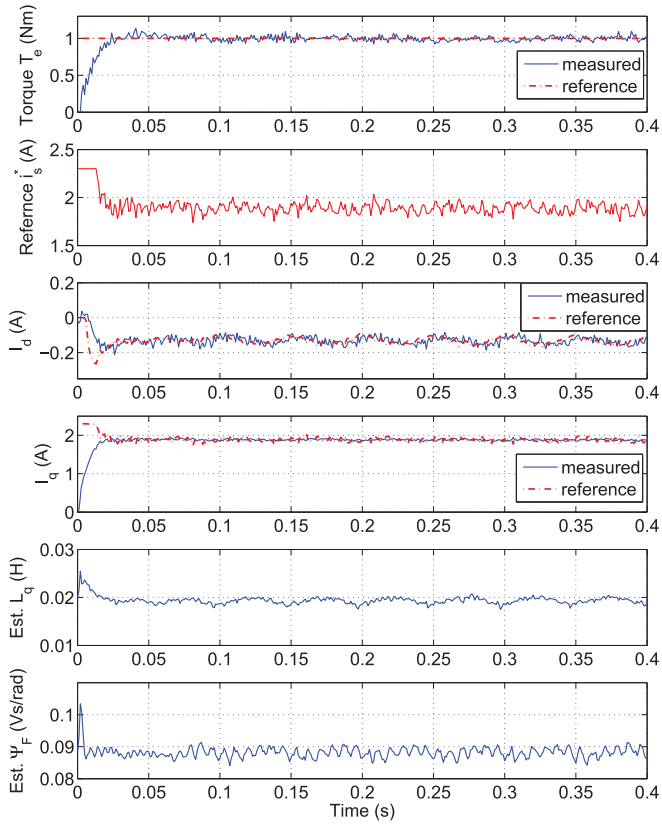

Fig. 8. Experimental results with $L_{q0} = L_q$ and $\psi_{F0} = \psi_F$ at $T_e^* = 1$ Nm.

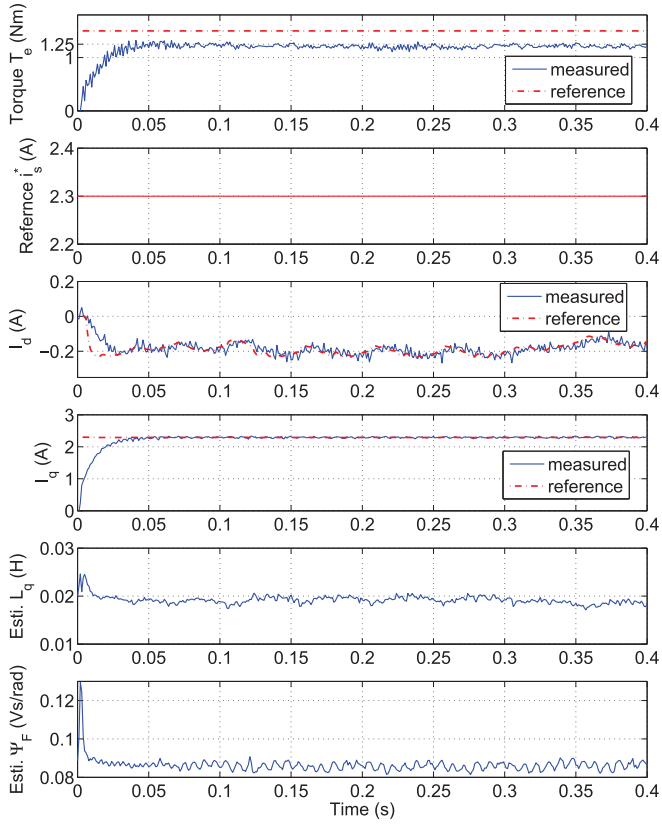

Fig. 9. Experimental results with $L_{q0} = L_q$ and $\psi_{F0} = \psi_F$ at $T_e^* = 1.5$ Nm.

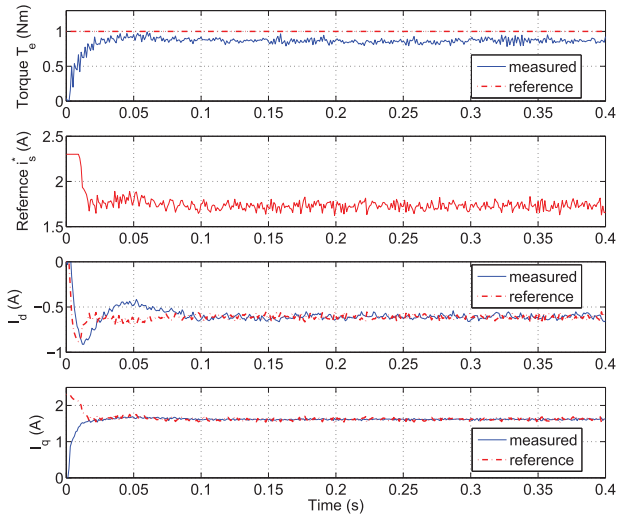

Fig. 10. Experimental results with $L_{q0} = 40$ mH at $T_e^* = 1$ Nm and without online parameter estimation.

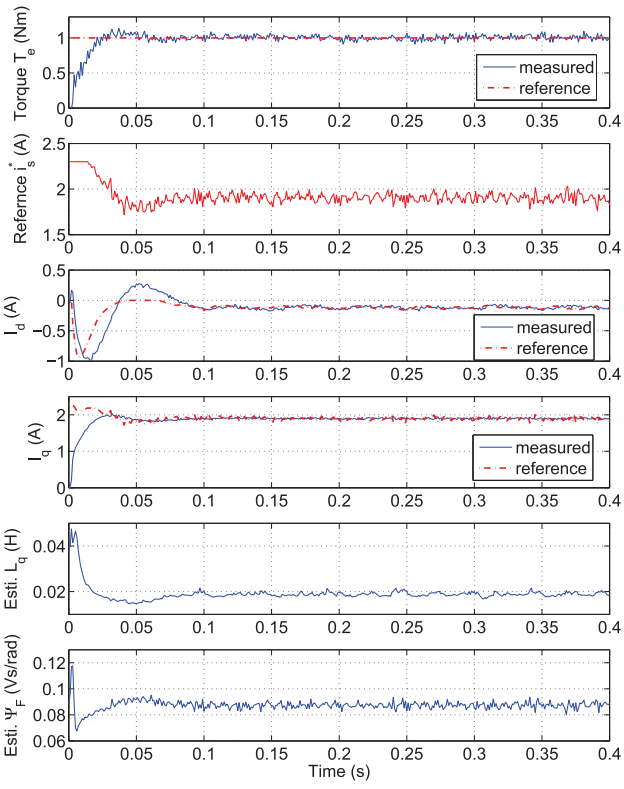

Fig. 11. Experimental results with $L_{q0} = 40$ mH at $T_e^* = 1$ Nm.

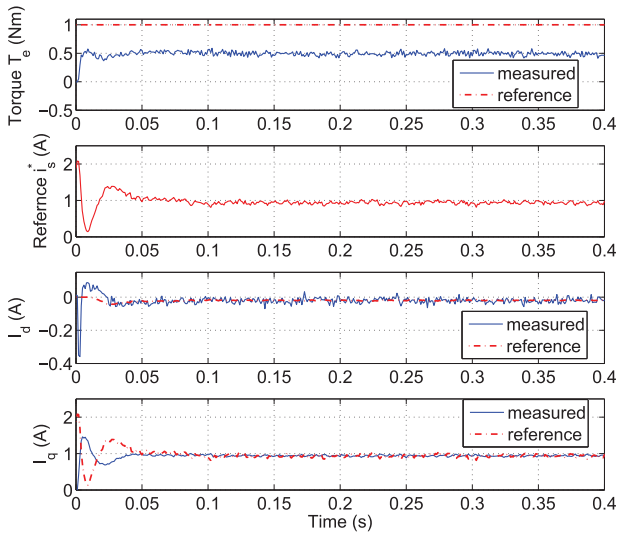

Fig. 12. Experimental results with $\psi_{F0} = 0.1772$ Vs/rad at $T_e^* = 1$ Nm and without online parameter estimation.

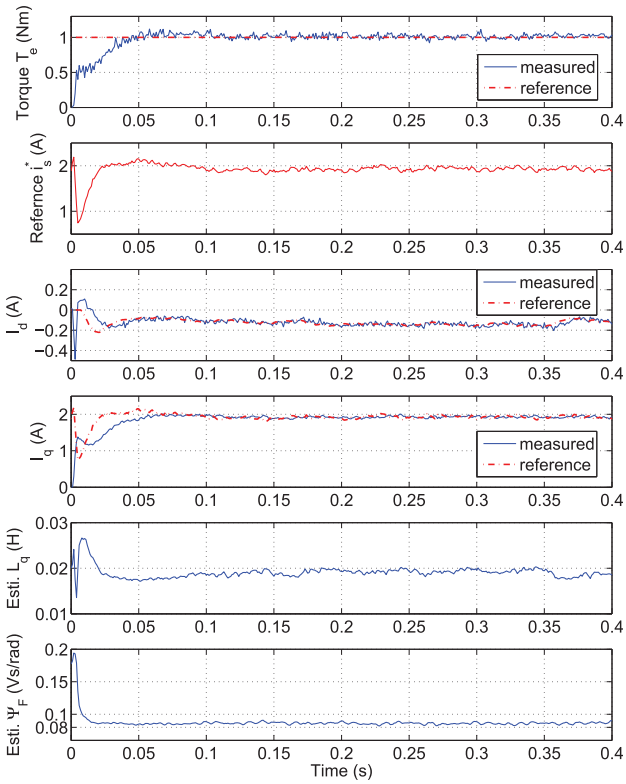

Fig. 13. Experimental results with $\psi_{F0} = 0.1772$ Vs/rad at $T_e^* = 1$ Nm.

safe for the implementation. However, with the parameter error, the operating point of the IPMSM deviates from the real MTPA condition, which results in steady state torque error. In Fig. 11, when with the online parameter estimation, the torque T_e of the IPMSM approaches to the reference value 1 Nm. No steady state error exists between T_e and T_e^*. Moreover, the estimated L_q is 19 mH at $i_q = 1.89$ A and the estimated ψ_F is 0.0877 Vs/rad, which is approximately the same as the one in Fig. 8. It indicates that the IPMSM operates closely around the optimum MTPA point. The estimated parameters converge to the real values within 50 ms. When compared to Fig. 8, the error of the q-axis inductance only has slight influence on the transient dynamics on the current reference i_s^* and the torque T_e.

Figs. 12 and 13 show the experimental results at 1 Nm with parameter error $\psi_{F0} = 0.1772$ Vs/rad, which is approximately double of the real flux linkage ψ_F. When without parameter estimation and with the wrong flux linkage, the torque deviates from the reference value. However, the PMSM drive system is still stable and the torque response is still smooth, which shows the safety and robustness of the proposed torque correction scheme.

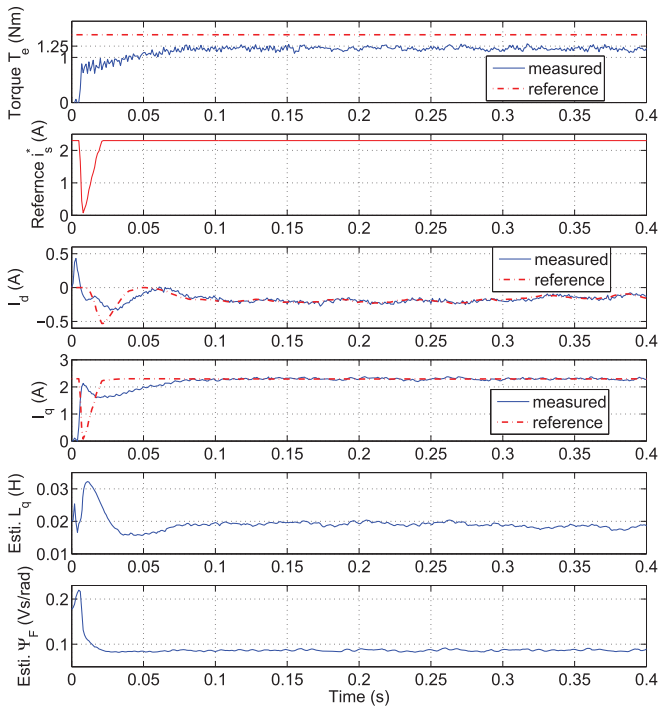

Fig. 14. Experimental results with $\psi_{F0} = 0.1772$ Vs/rad at $T_e^* = 1.5$ Nm.

With the online parameter estimation, the estimated L_q and ψ_F are stabilized within about 30 ms. The estimated L_q and ψ_F are 18.7 mH at $i_q = 1.9$ A and 0.875 Vs/rad respectively. The torque T_e of the IPMSM approaches to the reference value T_e^* and has mean value 1.01 Nm in steady state. The small steady state torque error is caused by the slight deviation of the estimated parameters, which can be resulted by the resistance increment. When compared to the transient dynamics for the no error case in Fig. 8, the convergence times of the current reference i_s^* and the torque T_e increase with the flux linkage error, which validates the analysis in Section IV-D with the doubling of ψ_{F0}. However, the steady state and the transient performance of the i_s^* and T_e are still satisfied.

The experimental results for the case of unreachable torque reference with parameter error $\psi_{F0} = 0.1772$ Vs/rad are shown in Fig. 14, where the reference torque is set to 1.5 Nm. It can be noticed that the PMSM drive system is safe and stable, while the current and torque stay at their maximum reachable values. The torque response is slowed down by the incorrect ψ_{F0} when compared to the one in Fig. 9 without flux linkage error. However, the transient torque response is still smooth. The estimated L_q and ψ_F are 18.7 mH and 0.0868 Vs/rad respectively.

VII. Conclusions

In this paper, an adaptive torque control scheme is introduced for an accurate and efficient torque control under MTPA condition. A self torque correction is designed, based on an ideal model of the IPMSM drive system without system uncertainty. The stability and performance of the proposed control scheme are theoretically proven for the ideal IPMSM drive system with known parameters and well controlled current loop. The current limitation is easily handled and no stability problem is evoked even the torque demand can not be reached. The proposed torque control scheme can be extended for the real IPMSM drive system with an adaptive current controller using MRAS and the online parameter estimation using RLS. For the implementation, the linear and nonlinear delay effects caused by the inverter and the DSP should be compensated in the controller. The resistance and the d-axis inductance can influence the accuracy of the torque and the MTPA operation. However, the influence is limited due to the feature of the IPMSM. The simulation and experimental results show the security, accuracy and robustness of the proposed control scheme with high performance.

APPENDIX

A. Proof of Lemma 3.1

In order to prove the convergence in Lemma 3.1, the torque reference is assumed as a constant without loss of generality. Taking the derivative of equation (16) and combining equation (14), the following equation can be obtained:

$$\tau^2 \Delta\ddot{T} + 2\tau\Delta\dot{T} = 2T_e^{'} - 2T_e^*. \tag{27}$$

Using equation (18) and $i_s^{'} = i_s^*$ without current limitation, equation (27) can be reformed into:

$$kp\psi_F\tau^2\dddot{i}_s^* + 2kp\psi_F\tau\ddot{i}_s^* + 2T_e^* = 2T_e^*. \tag{28}$$

Since $kp\psi_F\tau^2 << 2kp\psi_F\tau$, similar to the analysis in [21], the second order term in (28) can be removed according to the Singular Perturbation Approximation Principle. The simplified model can be described by the following equation:

$$\dot{i}_s^* = \frac{T_e^* - T_e^{'}}{kp\psi_F\tau}. \tag{29}$$

The transient dynamics of i_s^* in the real model (28) and the simplified model (29) have the negligible difference $\mathcal{O}(\tau)$. Furthermore, there is no steady state error between the real model and the simplified model. Denote the the partial derivative: $\frac{\partial T_e^{'}}{\partial i_s^*} = a(i_s^*)$. The torque $T_e^{'}$ and the current i_s^* have the same sign so that $a(i_s^*) > 0$. According the definition of the MTPA operation (15), the following relationship always holds:

$$|T_e^{'}| \geq 1.5p\psi_F|i_s^*|, \tag{30}$$

where equal holds if and only if $i_s^* = 0$ or $L_d = L_q$. Therefore, $a(i_s^*) \geq 1.5p\psi_F$ always holds. Considering the Lyapunov function $V(i_s^*) = \frac{1}{2}(T_e^* - T_e^{'})^2$, we have:

$$\dot{V}(i_s^*) = -\dot{T}_e^{'}(T_e^* - T_e^{'}) = -\frac{\partial T_e^{'}}{\partial i_s^*}\frac{di_s^*}{dt}(T_e^* - T_e^{'})$$

$$= -\frac{a(i_s^*)(T_e^* - T_e^{'})^2}{kp\psi_F\tau} \leq -\frac{2V(i_s^*)}{k\frac{\tau}{1.5}} \leq 0 \tag{31}$$

Therefore, the simplified system (29) as well as the real system (28) converge asymptotically to the invariant set $\{i_s^* : T_e^* - T_e^{'} = 0\}$. Since the torque $T_e^{'}$ is a strict monotonic function of i_s^*, i_s^* converges asymptotically to the unique solution of $T_e^{'} = T_e^*$, which is the MTPA operating point of the IPMSM. On the other hand, from eq. (31), it is also known that the torque error $T_e^{'} - T_e^*$ converges asymptotically to 0 with the convergence time faster than or equal to $k\frac{\tau}{1.5}$.

B. Cross coupling of test IPMSM

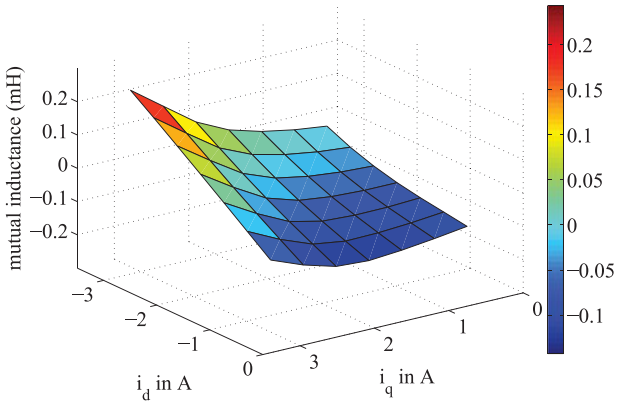

Fig. 15. Mutual inductance of the test IPMSM after 3D finite element analysis.

REFERENCES

[1] S.-Y. Jung, J. Hong, and K. Nam, "Current minimizing torque control of the IPMSM using ferraris method," *IEEE Trans. Power Electron.*, vol. 28, no. 12, pp. 5603–5617, Dec. 2013.

[2] G. Gallegos-Lopez, F. Gunawan, and J. Walters, "Optimum torque control of permanent-magnet AC machines in the field-weakened region," *IEEE Trans. Ind. Appl.*, vol. 41, no. 4, pp. 1020–1028, Jul. 2005.

[3] G. Rang, J. Lim, K. Nam, H.-B. Ihm, and H.-G. Kim, "A MTPA control scheme for an IPM synchronous motor considering magnet flux variation caused by temperature," in *Proc. 19th Annu. IEEE Appl. Power Electron. Conf. Expo.,* 2004, vol. 3, pp. 1617–1621.

[4] R. Ni, D. Xu, G. Wang, L. Ding, G. Zhang, and L. Qu, "Maximum efficiency per ampere control of permanent-magnet synchronous machines," *IEEE Trans. Ind. Electron.*, vol. 62, no. 4, pp. 2135–2143, Apr. 2015.

[5] A. Consoli, G. Scelba, G. Scarcella, and M. Cacciato, "An effective energy-saving scalar control for industrial IPMSM drives," *IEEE Trans. Ind. Electron.*, vol. 60, no. 9, pp. 3658–3669, Sep. 2013.

[6] S. Morimoto, M. Sanada, and Y. Takeda, "Effects and compensation of magnetic saturation in flux-weakening controlled permanent magnet synchronous motor drives," *IEEE Trans. Ind. Appl.*, vol. 30, no. 6, pp. 1632–1637, Nov. 1994.

[7] Y.-R. Mohamed and T. K. Lee, "Adaptive self-tuning MTPA vector controller for IPMSM drive system," *IEEE Trans. Energy Convers.*, vol. 21, no. 3, pp. 636–644, Sep. 2006.

[8] S.-J. Kim *et al.*, "Torque ripple improvement for interior permanent magnet synchronous motor considering parameters with magnetic saturation," *IEEE Trans. Magn.*, vol. 45, no. 10, pp. 4720–4723, Oct. 2009.

[9] S. Underwood and I. Husain, "Online parameter estimation and adaptive control of permanent-magnet synchronous machines," *IEEE Trans. Ind. Electron.*, vol. 57, no. 7, pp. 2435–2443, Jul. 2010.

[10] W. Huang, Y. Zhang, X. Zhang, and G. Sun, "Accurate torque control of interior permanent magnet synchronous machine," *IEEE Trans. Energy Convers.*, vol. 29, no. 1, pp. 29–37, Mar. 2014.

[11] C.-T. Pan and S.-M. Sue, "A linear maximum torque per ampere control for IPMSM drives over full-speed range," *IEEE Trans. Energy Convers.*, vol. 20, no. 2, pp. 359–366, Jun. 2005.

[12] H. Kim, J. Hartwig, and R. Lorenz, "Using on-line parameter estimation to improve efficiency of IPM machine drives," in *Proc. IEEE 33rd Annu. Power Electron. Spec. Conf.*, 2002, vol. 2, pp. 815–820.

[13] P. Niazi, H. Toliyat, and A. Goodarzi, "Robust maximum torque per ampere (MTPA) control of PM-assisted synrm for traction applications," *IEEE Trans. Veh. Technol.*, vol. 56, no. 4, pp. 1538–1545, Jul. 2007.

[14] K. Liu, Q. Zhang, J. Chen, Z. Zhu, and J. Zhang, "Online multiparameter estimation of nonsalient-pole PM synchronous machines with temperature variation tracking," *IEEE Trans. Ind. Electron.*, vol. 58, no. 5, pp. 1776–1788, May 2011.

[15] A. Wang, L. Zhang, and S. Dong, "Dynamic performance improvement based on a new parameter estimation method for IPMSM used for HEVs," in *Proc. 37th Annu. Conf. IEEE Ind. Electron. Soc.*, Nov. 2011, pp. 1825–1829.

[16] S. Bolognani, R. Petrella, A. Prearo, and L. Sgarbossa, "Automatic tracking of MTPA trajectory in IPM motor drives based on AC current injection," *IEEE Trans. Ind. Appl.*, vol. 47, no. 1, pp. 105–114, Jan. 2011.

[17] S. Bolognani, L. Peretti, and M. Zigliotto, "Online MTPA control strategy for DTC synchronous-reluctance-motor drives," *IEEE Trans. Power Electron.*, vol. 6, no. 1, pp. 20–28, Jan. 2011.

[18] S. Kim, Y.-D. Yoon, S.-K. Sul, and K. Ide, "Maximum torque per ampere (MTPA) control of an IPM machine based on signal injection considering inductance saturation," *IEEE Trans. Power Electron.*, vol. 28, no. 1, pp. 488–497, Jan. 2013.

[19] R. Antonello, M. Carraro, and M. Zigliotto, "Maximum-torque-per-ampere operation of anisotropic synchronous permanent-magnet motors based on extremum seeking control," *IEEE Trans. Ind. Electron.*, vol. 61, no. 9, pp. 5086–5093, Sep. 2014.

[20] T. Sun, J. Wang, and X. Chen, "Maximum torque per ampere (MTPA) control for interior permanent magnet synchronous machine drives based on virtual signal injection," *IEEE Trans. Power Electron.*, vol. 30, no. 9, pp. 5036–5045, Sep. 2015.

[21] Q. Liu and K. Hameyer, "An adaptive torque controller with MTPA for an IPMSM using model based self-correction," in *Proc. 40th Annu. Conf. Ind. Electron. Soc.*, Oct. 2014, pp. 391–397.

[22] Y. A. R. I. Mohamed and E. El-Saadany, "A current control scheme with an adaptive internal model for torque ripple minimization and robust current regulation in PMSM drive systems," *IEEE Trans. Energy Convers.*, vol. 23, no. 1, pp. 92–100, Mar. 2008.

[23] Q. Liu, A. Thul, and K. Hameyer, "A robust model reference adaptive controller for the PMSM drive system with torque estimation and compensation," in *Proc. 2014 Int. Conf. Elect. Mach.*, Sep. 2014, pp. 665–671.

[24] T. Nussbaumer, M. Heldwein, G. Gong, S. Round, and J. Kolar, "Comparison of prediction techniques to compensate time delays caused by digital control of a three-phase buck-type PWM rectifier system," *IEEE Trans. Ind. Electron.*, vol. 55, no. 2, pp. 791–799, Feb. 2008.

[25] G. Shen, W. Yao, B. Chen, K. Wang, K. Lee, and Z. Lu, "Automeasurement of the inverter output voltage delay curve to compensate for inverter nonlinearity in sensorless motor drives," *IEEE Trans. Power Electron.*, vol. 29, no. 10, pp. 5542–5553, Oct. 2014.

[26] P. Sergeant, F. De Belie, and J. Melkebeek, "Effect of rotor geometry and magnetic saturation in sensorless control of PM synchronous machines," *IEEE Trans. Magn.*, vol. 45, no. 3, pp. 1756–1759, Mar. 2009.

Qian Liu received the Bachelor's degree in electrical engineering from Shanghai Jiao Tong University, Shanghai, China, in 2008, and the Master's degree in control engineering from Technical University of Kaiserslautern, Kaiserslautern, Germany, in 2011. He is currently a Research Associate at the Institute of Electrical Machines, RWTH Aachen University, Aachen, Germany. His research interests include high performance PMSM drive system and power electronics in electrical vehicles and wind turbines.

Kay Hameyer (M'96–SM'99) received the M.Sc. degree in electrical engineering from the University of Hannover, Hanover, Germany, in 1986, and the Ph.D. degree from the University of Technology Berlin, Berlin, Germany, in 1992, for working on permanent magnet excited machines. After the university studies, he worked with the Robert Bosch GmbH in Stuttgart, Germany, as a Design Engineer for permanent magnet servo motors. From 1988 to 1993, he was a member of staff at the University of Technology Berlin. From 1996 to 2004, he was then a Full Professor of numerical field computations and electrical machines, Katholieke Universiteit Leuven, Leuven, Belgium. Since 2004, he has been a Full Professor and the Director of the Institute of Electrical Machines, RWTH Aachen University, Aachen, Germany. He has authored/coauthored more than 250 journal publications, more than 500 international conference publications, and four books. His research interests include all aspects of the design, control, and manufacturing of electrical machines and the associated numerical simulation, numerical field computation and optimization, the design and control of electrical machines, in particular, permanent-magnet excited machines, and induction machines. The characterization and modeling of hard- and soft-magnetic materials is another focus of his work. Since 2004, he has been a member of the German VDE, and since 2002, a Fellow of the Institution of Engineering and Technology, U.K.